Primljen / Received: 12.2.2013.
Ispravljen / Corrected: 9.7.2013.
Prihvaćen / Accepted: 25.7.2013.
Dostupno online / Available online: 10.9.2013.

Spatial dynamics of actual daily evapotranspiration

Author:

Bojana Horvat, PhD. CE
Hrvatske vode
Water Management Insitute
bojana.horvat@voda.hr

Original scientific paper

Bojana Horvat

Spatial dynamics of actual daily evapotranspiration

Estimation of actual daily evapotranspiration was conducted using SEBAL methodology, an approach based on surface energy balance equation that uses information derived from satellite image (NOAA AVHRR) and meteorological measurements from selected gauging stations, measured at the time of the satellite overpass. Apart from quantifying actual daily evapotranspiration, presented approach enables an insight into spatial characteristics of all energy balance components as well as spatial dynamics of evapotranspiration.

Key words:
actual daily evapotranspiration, SEBAL, surface energy balance, satellite image, meteorological measurements, spatial dynamics

Izvorni znanstveni rad

Bojana Horvat

Prostorna dinamika efektivne dnevne evapotranspiracije

Za procjenu efektivne dnevne evapotranspiracije odabran je SEBAL metodološki pristup koji se temelji na jednadžbi površinske energetske bilance, a kao ulazne podatke koristi informacije izvedene iz satelitskog snimka (NOAA AVHRR) te meteorološka mjerenja s odabranih meteoroloških postaja na dan preleta satelita. Ovim je pristupom, osim kvantifikacije efektivne dnevne evapotranspiracije, omogućen i uvid u prostorne značajke svih komponenata energetske bilance te prostornu dinamiku evapotranspiracije.

Ključne riječi:
efektivna dnevna evapotranspiracija, SEBAL, površinska energetska bilanca, satelitski snimak, meteorološka mjerenja, prostorna dinamika

Wissenschaftlicher Originalbeitrag

Bojana Horvat

Räumliche Dynamik effektiver Tagesevapotranspiration

Um die effektive Tagesevapotranspiration zu beurteilen, ist das auf der Gleichung täglicher Oberflächenenergiebilanz beruhende methodische Vorgehen SEBAL angewandt worden, das Daten aus Satellitenaufnahmen (NOAA AVHRR) und Messungen ausgewählter meteorologischer Stationen am Tag des Satellitenüberflugs als Eingangsparameter verwendet. Mit diesem Vorgehen ist, neben der Quantifikation der effektiven Tagesevapotranspiration, die Erläuterung räumlicher Merkmale aller Komponenten der Energiebilanz, sowie der räumlichen Dynamik der Evapotranspiration, ermöglicht.

Schlüsselwörter:
effektive Tagesevapotranspiration, SEBAL, Oberflächenenergiebilanz, Satellitenaufnahmen, meteorologische Messungen, räumliche Dynamik

1. Introduction

Mankind faces three fundamental problems in terms of water: too much water, too little water, and polluted water [1]. The problems have become more pronounced in recent years: hydrological extremes, droughts in particular, are becoming more frequent, while the quality of water has been degraded by inadequate water management practices. The evapotranspiration (ET) plays a crucial role during droughts since great amounts of water are being returned to the atmosphere, causing significant losses from the observed hydrological system. Complex and very variable, ET consists of two intricate processes that are difficult to analyze separately: evaporation (evaporation from free water surfaces, bare ground or from vegetation or objects on the earth's surface), and transpiration (physiological process of water transforming into water vapour through stomata) [2]. Numerous factors affect ET, the major ones being [3]: *water supply* (depth at which the water content is considered must be proportional to the root zone), *available energy* (ET will take place in proportion to available energy), *saturation deficit* (humidity index characterized by the difference between maximum and actual water vapour pressure of the volume of air), *turbulence transport* (if water vapour transfer into the atmosphere is stopped, the wetness gradient will decrease as well as the ET rate) and *stomatal conductance* (the key mechanism that takes into consideration the influence of vegetation on the ET process). Different characteristics of ecosystems will induce different intensity of influence of the described factors. That is one of the reasons why ET is the most difficult water balance component to estimate, while measurements are expensive and time consuming. The process will take place if three fundamental conditions are met [4]:

- continuous water supply,
- available energy needed for water to change from liquid to water vapour,
- water vapour gradient needed to enable water vapour flux from evaporative surface into the atmosphere.

Different methods are based on one or more of these conditions.

Simplest methods that have been proposed to estimate potential evapotranspiration use only monthly averages of air temperatures as input data (Blaney and Criddle, 1950; Thornthwaite, 1948; Hamon, 1961), while more complex ones take into the consideration solar radiation, humidity, wind velocity, and characteristics of vegetation cover (Jensen and Haise, 1963; Turc, 1954, Penman, 1948). Numerous scientists have continued to develop the Penman's method and introduced in this respect two new input parameters – aerodynamics and surface resistance. The method went through numerous modifications, the best known being the Monteith's modification (Monteith, 1965). The Makkink's model (Makkink, 1957) and the Priestly-Taylor method (1972) are also widely used. Many authors have investigated and compared currently available methods (e.g. [5, 6]). However, none of these methods have been accepted as the most accurate for estimating evapotranspiration of an area.

Direct measurements of actual evapotranspiration are often being conducted using an evaporation pan, though such measurements are not representative with regard to the influence of vegetation on moisture losses. Lysimeters are also widely used but the measurements are time consuming and highly expensive. Thus the most common approach has been the application of analytical and empirical equations developed to estimate correlation between measured evapotranspiration and climatologic data that directly or indirectly influence ET. Satellite technology developments over the past decades have enabled introduction of new methods, which are based on information derived through remote sensing. The complexity of the methods lies in the relationship between the empirical and physical, and it is difficult to classify them unambiguously. Most of them are based on the surface energy budget. One of main advantages of remote sensing based methods is not only in estimating quantitative relation between energy balance components, but also in their ability to provide an insight into their spatial structure and hence spatial variability of ET, which is extremely important for the understanding of water balance in a particular area (whether it be a catchment, administrative unit, continent, etc.).

2. Mathematical model for estimating evapotranspiration

Baastiansen et al. [7] formulated the Surface Energy Balance for Land (SEBAL) algorithm to estimate the actual daily evapotranspiration using data derived from remote sensing and meteorological data measured at gauging stations. The analysis of standard and available satellite images described in the model is based on physical principles and requires minimum ancillary data from meteorological gauging stations, which makes the method convenient for regions with sparse data. Surface parameters (surface albedo, vegetation indices, and surface temperature) are estimated using the spectral information derived from chosen sensor in the visible, near infrared (IR) and thermal infrared (TIR) part of the electromagnetic spectrum, and converted to surface energy balance components. In the last step, various moisture indicators (e.g. evaporative fraction) are calculated.

The model is based on the fact that evaporation can only take place if sufficient amount of energy is available, and so the process is bound by the available energy [8]. With that limitation, the evapotranspiration can be estimated by applying the energy conservation principle: energy that reaches the earth's surface must be equal to the energy leaving the system within the same time interval. The surface energy balance is formulated using the equation for the surface net radiation R_n:

$$R_n = \lambda ET + G_0 + H \quad (1)$$

where G_0 stands for the soil heat flux i.e. the heat flux in, through, and from the soil, H is the sensible heat flux i.e. the heat flux between the surface and the atmosphere, while λET represents

the latent heat flux, which is the energy necessary for water to change from liquid to water vapour. The equation (1) deals with four main energy balance components only, and neglects the remaining components that represent only a small portion of the daily net radiation and hence are significantly smaller in comparison with the four main components.
Components R_n, G_0 and H can be measured directly, while λET is estimated as a residual from the equation (1). However, direct measurements of R_n, G_0 and H are usually not available since the measurements require complex and expensive equipment and are time consuming. Remote sensing enables indirect measurement of these three energy balance components, based on a quick and simple access to necessary information. This method greatly reduces time needed to estimate ET.

2.1. Net radiation (Rn)

The net radiation is a function of incoming and outgoing radiation and can be measured by the net radiometer. However, the measurements are scarce and usually unavailable, which is why the net radiation is calculated using the surface reflectance i.e. broadband surface albedo α_0 and surface temperature T_0, as well as spatially variable zenith angles (to account for the spatially variable incoming shortwave radiation). In general, the net radiation is calculated using the equation [9]:

$$R_n = (1 - \lambda_o) \cdot K\downarrow + L\downarrow - L\uparrow \ [W/m^2] \quad (2)$$

where α_0 is the broadband surface albedo, $K\downarrow$ is the incoming shortwave radiation, $L\downarrow$ is the incoming longwave radiation, and $L\uparrow$ is the outgoing longwave radiation.
The instantaneous incoming shortwave radiation $K\downarrow$, and the instantaneous incoming longwave radiation $L\downarrow$ are dependent on the geometry and meteorological data measured at gauging stations. In that respect, they are estimated as point values, at discrete locations of meteorological gauging stations.
The incoming shortwave radiation $K\downarrow$ depends on the geometry and atmospheric factors: day of the year, latitude, insolation, and atmospheric constituents. The SEBAL defines it as a function of atmospheric transmittance τ_{sw} and instantaneous shortwave radiation at the top of the atmosphere $K\downarrow^{TOA}$ [9]:

$$K\downarrow = \tau_{sw} \cdot K\downarrow^{TOA} \ [W/m^2] \quad (3)$$

The atmospheric transmittance describes capacity of the atmosphere to transmit radiation and in this case is calculated using the altitude of selected gauging stations [9]. The instantaneous shortwave radiation at the top of the atmosphere is constant for the whole region and equal to maximum instantaneous shortwave radiation beyond the atmosphere (i.e. solar constant SC = 1367 W/m^2), corrected for the earth's eccentricity (correction eccentricity factor E_0) and solar zenith angle θ [9], thus resulting in 1039,33 W/m^2.

The longwave incoming radiation $L\downarrow$ refers to thermal radiation emitted by the atmosphere and atmospheric constituents. Its calculation is based on the Stefan-Boltzmann law: the instantaneous incoming longwave radiation is a function of the Stefan-Boltzmann constant σ ($\sigma = 5{,}67 \cdot 10^{-8}$ W/m^{2}K^4), air temperature T_a (K) measured at gauging stations, and the atmospheric emissivity ε_a:

$$L\downarrow = \sigma \cdot \varepsilon_a \cdot T_a^4 \ [W/m^2] \quad (4)$$

Unlike the incoming radiation, the spatial variability of the instantaneous outgoing longwave radiation $L\uparrow$ is significant as it refers to the thermal radiation emitted by the earth's surface. It can also be calculated by applying the Stefan-Boltzmann law, but is dependent on the surface temperature T_0 and the broadband surface emissivity ε_0 [9]:

$$L\uparrow = \varepsilon_0 \cdot \sigma \cdot T_0^4 \ [W/m^2] \quad (5)$$

The value of $L\uparrow$ depends on the parameters that are difficult to measure, but can be derived from the satellite image. The broadband surface emissivity depends on characteristics of the vegetation cover, expressed in form of the vegetation index NDVI (Normalized Difference Vegetation Index) [10]:

$$\varepsilon_0 = 1{,}0094 + 0{,}047 \cdot \ln(NDVI) = 1{,}0094 + 0{,}047 \cdot \ln\left(\frac{nearIR - red}{nearIR + red}\right) \quad (6)$$

The mathematical formulation of NDVI enables quantification of the vegetation i.e. its productivity. Its value domain ranges from -1 to 1: a dense and healthy vegetation will have positive values close to 1, while low positive or negative values of NDVI are typical for water surfaces. In other words, more radiation is reflected in the near IR wavelength range in comparison with the red band, which is an indication of denser vegetation and it often refers to some forest species. When the difference between near IR and red band is small, the surface is most likely covered with scarce and often dry vegetation.
In most models, the surface temperature is the boundary condition for energy balance. As opposed to air temperature measured 1,5 – 2 m above the ground at standard meteorological gauging stations, the surface temperature must be measured at the very surface. In this approach, the surface temperature is calculated using physical parameters that are directly derived from the bands of the chosen sensor. The calculation procedure consists of two steps:

Step 1: Brightness temperature is estimated for both TIR bands:

$$T_i = \frac{C_2 \cdot \nu_i}{\ln\left(1 + \frac{C_1 \cdot \nu_i^3}{L_i}\right)} \ [K] \quad (7)$$

where C_1 and C_2 are the constants characteristic for the chosen sensor, ν_i is the central wave number of the band (c/m), and spectral radiance L_i is a linear function of the 10-bit visible band count [11].

Step 2: Surface temperature is estimated using the split-window technique, in this case the Coll's equation [12]:

$$T_0 = T_4 + [1{,}29 + 0{,}28 \cdot (T_4 - T_5)] (T_4 - T_5) + 45 \cdot (1 - \varepsilon_4) - 40\Delta\varepsilon \text{ [K]} \quad (8)$$

where T_4 and T_5 represent brightness temperatures in bands 4 and 5, while ε_4 is the emissivity in the band 4, and $\Delta\varepsilon$ is the difference in emissivity between the bands 4 and 5.

The surface net radiation cannot be estimated if reflection characteristics of the surface are unknown. Such characteristics can be described by the broadband surface albedo α_0, a parameter referring to reflectance of the shortwave radiation in the wavelength interval 0,3 – 3 μm [13]:

$$\alpha_0 = \frac{\alpha_{TOA} - \alpha_{PR}}{\tau_{sw}^2} \quad (9)$$

where α_{TOA} is the planetary albedo (albedo at the top of the atmosphere) and α_{PR} is the path radiance i.e. an average portion of the incoming solar radiation across all bands of the chosen sensor, back-scattered to the sensor before it reaches the earth's surface, with the value range of 0,025-0,4 [7] . The planetary albedo is the sum of the narrowband reflectance (α_i) multiplied by adequate weighting factors (w_i) that are sensor dependent [14]:

$$\alpha_{TOA} = \sum_i w_i \cdot \alpha_i \quad (10)$$

2.2. Soil heat flux (G_0)

The soil heat flux is the amount of energy passing through the soil in a unit of time. The main driver is solar radiation which heats up the surface, creating the temperature difference between the surface and upper layers of the soil profile. The heat conductance in soil is analogous to heat conductance through the solid body. Hence the Fourier's law, according to which the transferred heat is proportional to the negative temperature gradient, can be applied:

$$G_0 = -\lambda_S \cdot \frac{\Delta T_S}{\Delta z} \text{ [W/m}^2\text{]} \quad (11)$$

where λ_S is the proportionality factor i.e. thermal conductivity (W/mK) and the ratio $\Delta T_s/\Delta z$ defines the vertical temperature gradient (K/m). The ability of soil to transfer heat determines how fast the temperature will change during a day or a season [15] while the temperature gradient governs the heat flux and is dependent on vegetation cover (heating rate of the surface is determined by the light attenuation and formation of shadows at the very surface).

Although the soil heat flux cannot be mapped directly from satellite imagery, appropriate methods have been developed for measuring soil temperature and one or more thermal characteristics of the soil (thermal conductivity or thermal capacity), as well as the water content. However, such approaches cannot adequately describe the spatial and temporal variability of the soil heat flux, primarily due to pronounced dynamic thermal characteristics of the surface and complex interrelationship between annual, seasonal and diurnal solar radiation regimes. Since the soil heat flux is a part of the net radiation, Baastiansen [16] has developed an algorithm that estimates the ratio G_0/R_n based on the surface temperature T_0 (K), broadband surface albedo α_0, and characteristics of the vegetation cover expressed in form of NDVI:

$$\frac{G_0}{R_n} = \left(\frac{T_0 - 273}{\alpha_0}\right) \cdot \left[0{,}0032 \cdot (1{,}1 \cdot \alpha_0) + 0{,}0062 \cdot (1{,}1 \cdot \alpha_0)^2\right] \cdot (1 - 0{,}978 \cdot NDVI^4) \quad (12)$$

2.3. Sensible heat flux (H)

The sensible heat flux between the surface and the atmosphere is a measure of energy loss from the soil through processes of convection and diffusion, and is triggered by the temperature difference between the surface and the atmospheric surface layer. Calculations are based on the theory of heat transport between the earth's surface and the surface layer of the atmosphere. Hence, H is proportional to the difference between the air temperature and the surface temperature ($T_0 - T_a$) and inversely proportional to the aerodynamic resistance to heat transport r_{ah} [7]:

$$H = \rho_a \cdot c_p \cdot \frac{T_o - T_a}{r_{ah}} \text{ [W/m}^2\text{]} \quad (13)$$

where ρ_a is the air density (kg/m^3), c_p is the specific heat of the air (1004 J/kgK), and r_{ah} is the aerodynamic resistance to heat transport (s/m).

The third component of the energy balance equation, the sensible heat flux, is the most complex part in estimating evapotranspiration, and is very difficult to estimate. Firstly, it is not possible to directly measure parameters that r_{ah} depends on and, secondly, the data necessary to estimate those parameters are usually unavailable. Therefore, the aerodynamic resistance to heat transport is estimated in an iteration process, as schematically shown in Figure 1.

Knowing the wind velocities u measured at the height z above the ground at the time of the satellite overpass, the roughness length for momentum is estimated as a function of vegetation height and displacement height [17]:

$$z_{0m} = \gamma \cdot (h_0 - d) \quad (14)$$

Where $\gamma = 0{,}2$, h_0 is the vegetation height and d is the zero plane displacement (displacement height), i.e. an average level at which momentum is absorbed due to vegetation. Raupach [18] connects d with vegetation cover defining it as a function of the leaf area index LAI. With known roughness length for momentum, and assuming neutral atmospheric conditions, it is possible to calculate the friction velocity at gauging stations, at $z = 2$ m above the ground:

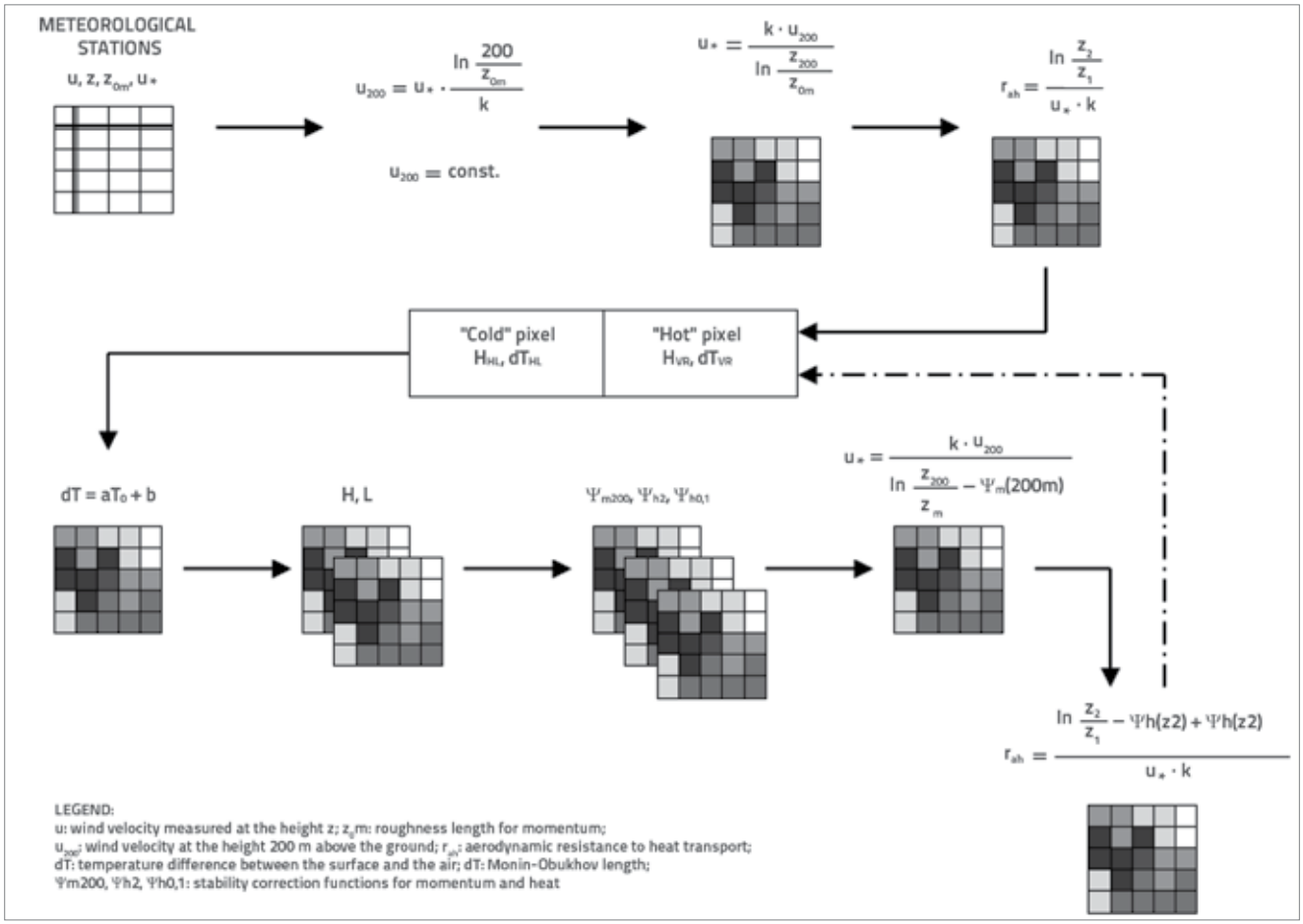

Figure 1. Schematic overview for calculating sensible heat flux *H*

$$u_* = \frac{k \cdot u}{\ln \frac{z}{z_{0m}}} \tag{15}$$

The blending height defines the height at which the surface roughness influence can be neglected. In this case, it is 200 m above the ground (surface roughness is a part of the vegetation height that influences shear stress between the plant and the atmosphere and defines surface flux as well as the actual and potential evapotranspiration). At that height, the wind velocity is assumed to be constant for the whole region, and is calculated as a function of friction velocity and roughness length for the momentum:

$$u_{200} = u_* \cdot \frac{\ln \frac{200}{z_{0m}}}{k} \tag{16}$$

Initial values of aerodynamic resistance to heat transport are determined in every pixel of the analyzed area, assuming neutral stability [8, 19, 20]:

$$r_{ah} = \frac{\ln \frac{z_2}{z_1}}{u_* \cdot k} \tag{17}$$

where z_1 is the height above d of the vegetation ($z_1 \approx 0{,}1$ m), z_2 is the height below the surface layer ($z_2 \approx 2$ m), u_* denotes the friction velocity (m/s), and k stands for the von Karman's constant (0,41). To estimate the temperature difference between the surface and the air for the analyzed area, $dT = T_0 - T_a$ the function $dT = T_0 - T_a$ must be defined. The procedure starts by defining two boundary conditions: the known sensible heat flux at extremely wet ("cold" pixel) and extremely dry spot i.e. pixel ("hot" pixel). The "cold" pixel usually represents an open water surface where $H \approx 0$, i.e. all available energy is used in the evaporation process, and hence $R_n - G_0 = \lambda ET$. If open water surfaces can not be detected, the most accurate choice is a well irrigated pixel characterized with dense vegetation, albedo in the range of 0,22 – 0,24, high NDVI and low surface temperature. If $H \approx 0$, according to equation (13), the temperature difference between the surface and the air is equal to zero: $dT_{HL} = T_{0HL} - T_{aHL} = 0$. As opposed to "cold" pixel, $\lambda ET \approx 0$ and $H = R_n - G_0$. can be assumed for "hot" pixel. The surface temperature is at maximum value, while the NDVI and albedo are very low. Since the values of R_n, G_0 and r_{ah} are already known from previous steps (equations (2), (12) and (17)), temperature differences between the surface and the air are calculated by inversing the equation (13). The resulting values enable defining the

linear function dT (Figure 2), which is then applied to the whole analyzed area, i.e. to every pixel.

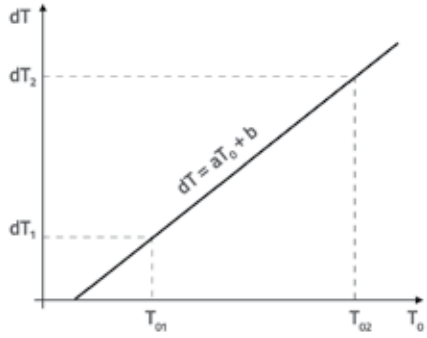

Figure 2. Temperature difference between the surface and the air

The equation (13) determines the sensible heat flux and the Monin-Obukhov length, which represents the ratio between the turbulence generated mechanically and thermally [21]:

$$L = -\frac{\rho \cdot c_p \cdot u_*^3 \cdot T_0}{k \cdot g \cdot H} \tag{18}$$

with ρ as the air density [kg/m³], c_p is the specific heat of the air [1004 J/kgK], u_* is the friction velocity [m/s], T_0 is the surface temperature [K], g is the gravitational acceleration [9,81 m/s²] and H is the sensible heat flux [W/m²]. In unstable conditions, when L<0, the boundary layer is approaching the state of free convection where buoyancy processes are dominant. When conditions are stabile (L>0), the vertical movement of turbulent eddies is bounded by the stratification. Hence, turbulent eddies are limited by the stability, rather than by the distance from the ground [21]. In neutral conditions, the Monin-Obukhov length equals zero (L=0).

2.4. Latent heat flux (λET)

The latent heat flux is a measure of heat loss from the surface through the evapotranspiration process and is estimated as a residue of the surface energy balance, based on equation (1). It must be emphasized that the estimated latent heat flux represents the instantaneous value i.e. the value at the time of the satellite overpass. Accordingly, the instantaneous ET can be calculated by dividing the latent heat flux by the latent heat of vaporization λ.

2.5. Actual daily evapotranspiration (ET_{24h})

To estimate the actual daily evapotranspiration, its diurnal variation must be known, which is similar to variation of other energy balance components [9]. Knowing the instantaneous evaporation and variation of one of the surface energy balance components, it would be possible to estimate diurnal variation of evaporation assuming that the relative distribution of energy flux between the main components remains the same. If the assumption is valid, the evaporative fraction Λ, i.e. the ratio between the latent λET and available energy $R_n - G_0$ is constant during the day [22, 23, 24] and $\Lambda_{INSTANTANEOUS} = \Lambda_{24h} = \Lambda$. In that case, the actual daily evapotranspiration ET_{24h} is a function of the daily net radiation R_{n24h} and evaporative fraction Λ [7]:

$$ET_{24h} = \frac{8{,}64 \cdot 10^7 \cdot \Lambda_{INSTANTANEOUS} \cdot R_{n24h}}{\lambda \cdot \rho_w} = \frac{\Lambda \cdot R_{n24h}}{28{,}588} \tag{19}$$

where ρ_w is the density of water (ρ_w = 1000 kg/m³). The latent heat of vaporization λ expresses the energy needed to change the unit mass of water from liquid into water vapour under constant pressure and at constant temperature. It is temperature dependent and hence its value will change as the temperature changes: at higher temperatures less energy is needed to evaporate water. On the other hand, the variation of λ with respect to the temperature is small enough to be neglected and its values can be assumed constant and equal to 2,47 MJ/kg [8], which corresponds to air temperature of app. 20°C.

3. Research area

The actual daily evapotranspiration was estimated at the Croatian part of the Istrian Peninsula (Figure 3.a). Covering the area of app. 3.160 km², it is the largest peninsula in the Adriatic. The northern boundary stretches from Mugglia (Italy) to Preluka located in the Kvarner Bay (Croatia). Although relatively small, the Istrian Peninsula is very heterogeneous. The relief in the western and southern parts is more or less monotonous but develops rapidly towards the north and the north-east, reaching the altitude of 1.402 m a.s.l. The complex hydrogeology of the area is causing inhomogeneous hydrology: the surface hydrographic network is well developed only in a smaller portion, while the rest of the peninsula is characterized by the karstic underground hydrographic network and numerous karstic springs [25].

The Mediterranean climate prevails in coastal parts where summers are hot and dry while winters are moderately cold and wet. As the distance from the coast and the altitude increase, weather conditions gradually change into moderate continental: warm and wet summers and cold winters. Average annual air temperatures in the coastal area exceed 15°C and decrease towards the mainland down to the minimum of 6-7°C at the Učka and Ćićarija mountain ranges [26]. Lower altitudes and a monotonous relief are found in the west and south, where air temperatures are, on an average, significantly higher compared to the rest of Istria, and the vertical gradient is not so pronounced (Figure 3.b).

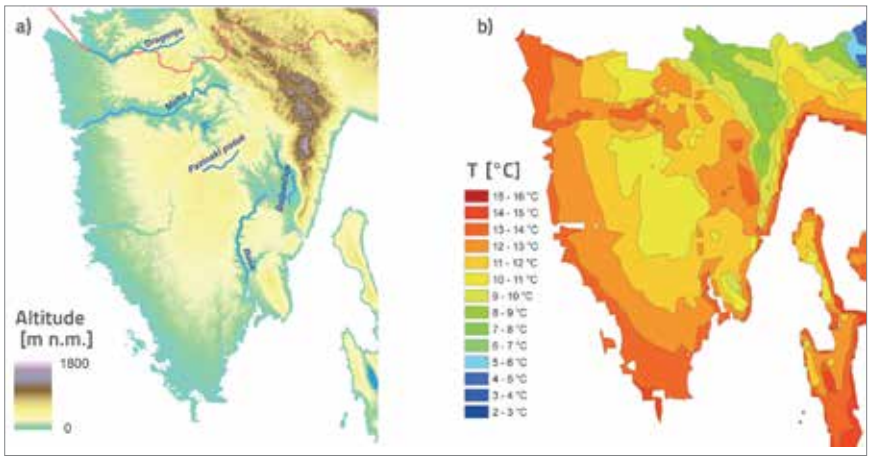

Figure 3. a) Analyzed area; b) spatial distribution of average annual air temperatures in the period of 1961-1990. [26]

Figure 5. Meteorological gauging stations selected in the analyzed are

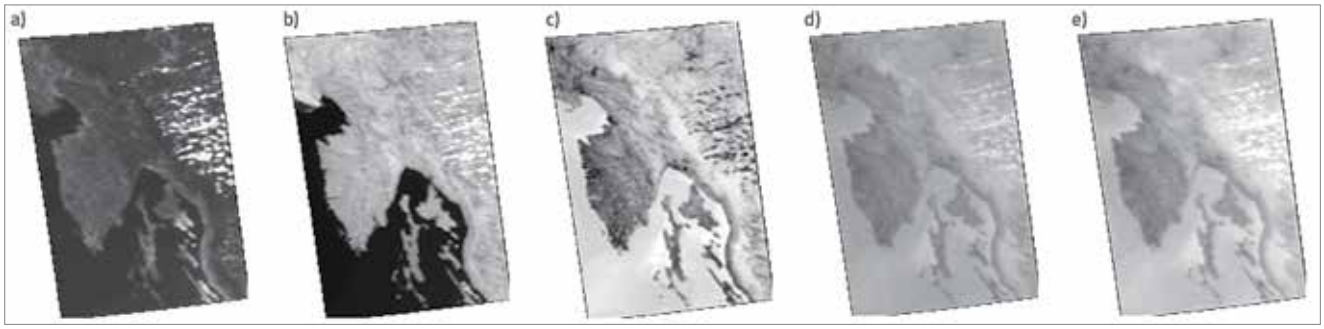

Figure 4. NOAA AVHRR satellite image taken on 5th August 1998 at 13:55 h: a) band 1 (0,58 – 0,68 μm); b) band 2 (0,725 – 1,10 μm); c) band 3 (3,55 – 3,93 μm); d) band 4 (10,30 – 11,30 μm); e) band 5 (11,50 – 12,50 μm)

4. Input data and satellite image

The satellite image chosen for estimating the actual daily evapotranspiration was NOAA (National Oceanic and Atmospheric Administration) AVHRR (Advanced Very High Resolution Radiometer), taken on 5th August 1998 at 13:55 h (Figure 4). It consists of 5 bands, each covering a specific interval in EMS. Along with the image, meteorological data were also collected at 11 selected meteorological gauging stations, where the following measurements were made at the time of the satellite overpass: air temperature, relative air humidity, insolation and wind velocity (Figure 5).

5. Results and discussion

Using equations (3) and (4), $K\downarrow$ and $L\downarrow$ were calculated for each meteorological station (table 1)..

Table 1. Instantaneous incoming shortwave K↓ and longwave L↓ radiation

Stations	τ_{sw}	ε_a	K↓ [W/m²]	L↓ [W/m²]
Abrami	0,752	0,759	781,26	354,81
Celega	0,750	0,760	779,91	350,31
Cres	0,750	0,760	779,60	350,35
Ćepić	0,751	0,760	780,12	350,28
Labin	0,755	0,758	784,90	344,05
Pazin	0,756	0,758	785,54	343,04
Poreč	0,750	0,760	779,81	353,13
Pula	0,751	0,760	780,39	353,05
Pula aerodrom	0,751	0,759	780,80	348,32
Rijeka	0,752	0,759	781,99	346,30
Rovinj	0,750	0,760	779,91	351,71

τ_{sw}: one-way atmospheric transmittance ($\tau_{sw} = 0{,}75+2\cdot10^{-5}\cdot z$); ε_a: atmospheric emissivity ($\varepsilon_a = 0{,}85 \cdot (-\ln \tau_{sw})^{0{,}09}$)

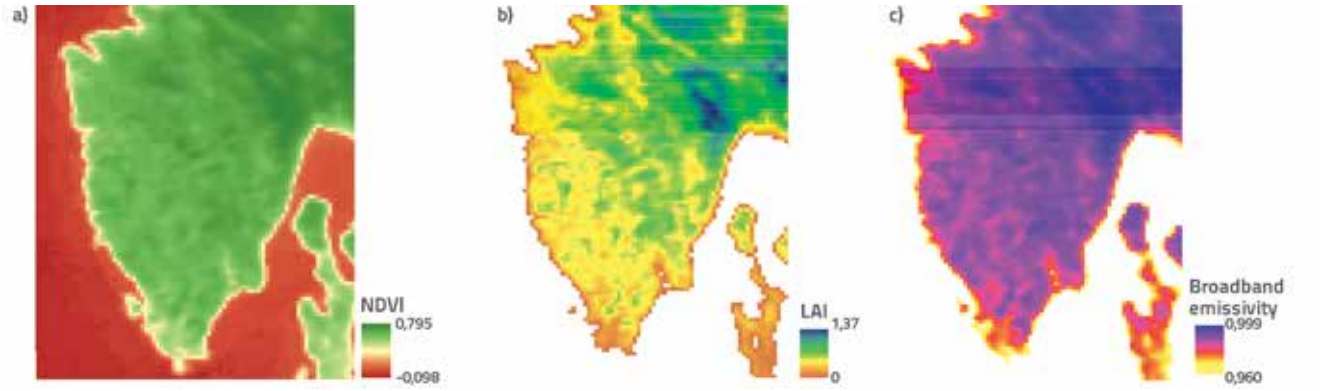

Figure 6. a) Vegetation index NDVI; b) leaf area index LAI; c) broadband emissivity

Spatial variations of instantaneous incoming shortwave and longwave radiation are very small over the analyzed area ($K\downarrow$ = 779,60 – 785,54 W/m^2; $L\downarrow$ = 343,04 – 353,13 W/m^2) and can be assumed to be constant and equal to their average value ($K\downarrow$ = 781,29 W/m^2 and $L\downarrow$ = 349,58 W/m^2).

Vegetation indices NDVI and LAI are higher in the north and north-east parts of Istria (Figures 6.a and 6.b), which implicates a dense and healthy vegetation (forest species), but they decrease towards the western and southern coast where dry and scarce vegetation prevails. The broadband emissivity (Figure 6.c) will increase as the NDVI increases: higher values are characteristic for the central peninsula as well as the north and north-east.

The surface temperature (Figure 7) is a function of thermal characteristics of the surface, which are, among other factors, dependent on vegetation cover. Higher surface temperatures are detected in areas with no or with very scarce and dry vegetation that predominate in coastal parts of the peninsula, i.e. in areas with low NDVI and LAI values (Figure 6.a and Figure 6.b), while lower temperatures are present in the north, which is covered with dense vegetation. Having roots deep in the ground, trees can reach groundwater all year long. In this way, the transpiration process, which requires a great amount of energy, can be conducted even during droughts while only a smaller portion of that energy is used to heat-up the surface and hence surface temperatures are lower.

Using the equation (5), maximum values of instantaneous outgoing longwave radiation $L\uparrow$ are calculated for the west and south coast of the analyzed area (Figure 8) where surface temperatures are the highest. The decrease in $L\uparrow$ is proportional to the decrease in surface temperatures.

The instantaneous net radiation of the analyzed area is determined using equation (2) (Figure 9).

With known instantaneous net radiation, the equation (12) is used to calculate a portion of the net radiation related to the soil heat flux i.e. spatial distribution of G_0 (Figure 10).

Maximum values of G_0 are registered in the coastal area, especially in the west and south. Sparse vegetation cover in those parts results in an increased energy flux that passes through the soil. Denser and healthier vegetation (higher NDVI values) contributes to the light attenuation on the surface and reduces the soil heat flux.

Depending on the value of L, the friction velocity is calculated and adjusted using stability correction functions [27] before estimating the aerodynamic resistance to heat transfer (Figure 1). After 11 iterations, H and r_{ah} values stabilize, and the final spatial distribution of sensible heat flux is determined (Figure 11).

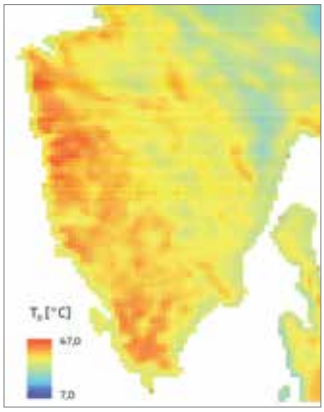

Figure 7. Surface temperature (5th August 1998)

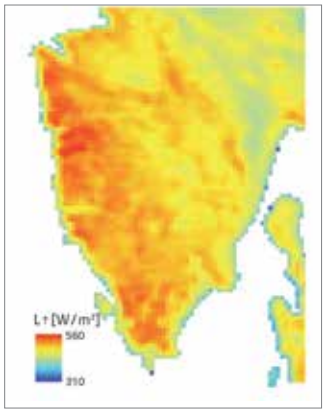

Figure 8. Instantaneous outgoing lw radiation (5th August 1998)

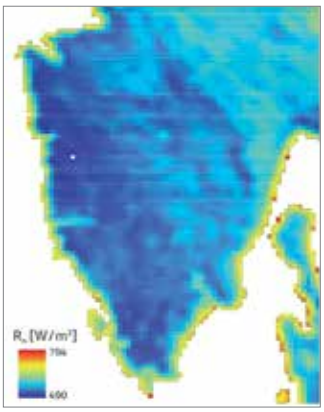

Figure 9. Instantaneous net radiation (5th August 1998)

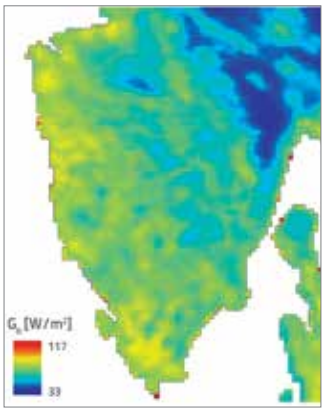

Figure 10. Instantaneous soil heat flux (5th August 1998)

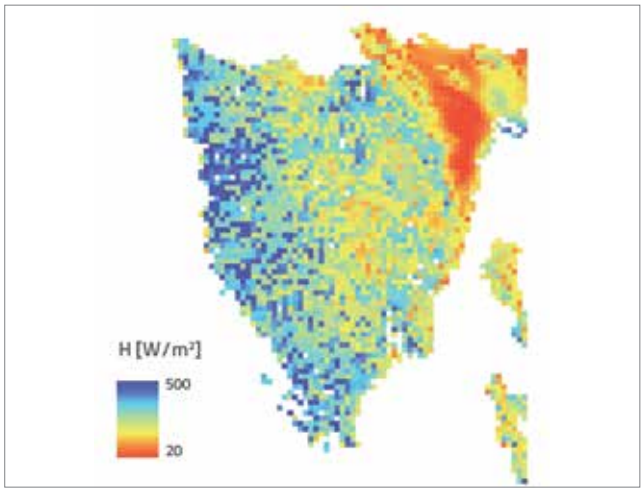

Figure 11. Instantaneous sensible heat flux (5 August 1998)

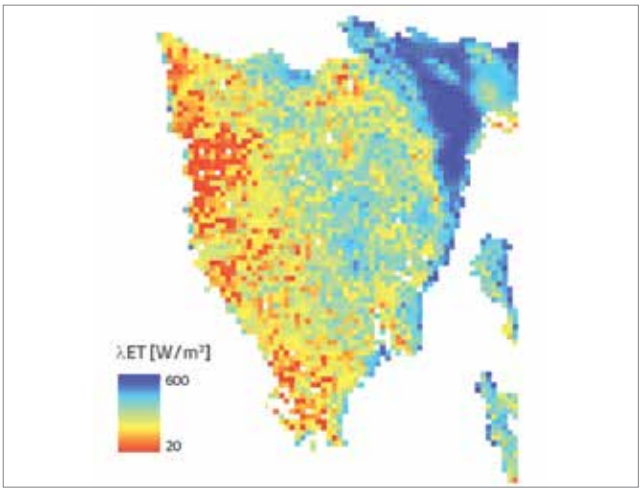

Figure 13. Instantaneous latent heat flux (5 August 1998)

The lowest values of sensible heat flux are found in the north-east part of the peninsula where surface temperatures are also the lowest. Hence, the loss rate of energy from the soil will also be equal to minimum values (Figure 12). An increase in surface temperature will result in an increase in sensible heat flux, and so high values of H (above 400 W/m^2) have been recorded at several locations in the western and southern parts of Istria. The heat loss is significant in these locations, and high values are in line with high values of the soil heat flux (Figure 10). Large amounts of available energy are spent on rising soil temperature, and heat transfer into the atmosphere is significant. It is obvious that available energy is mainly used for heating-up the surface, which means that less energy is available for changing water from liquid to water vapour, i.e. for the evapotranspiration process.

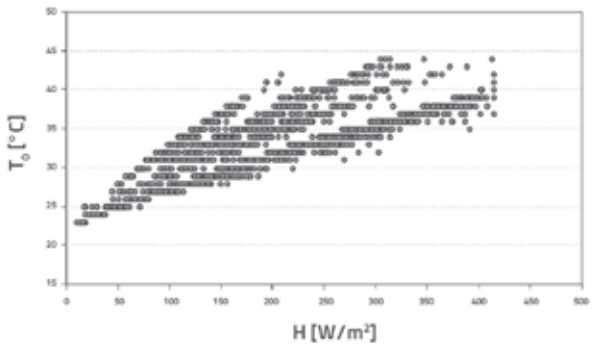

Figure 12. Relationship between sensible heat flux and surface temperature

The process of transferring heat from surface into the atmosphere is complex and depends on numerous factors, and so greater dispersion of sensible heat flux values occurs when surface temperatures are higher (Figure 12).

The latent heat flux is the energy elapsed in the ET process. Knowing the energy balance components as well as their spatial distribution, the λET can be determined as a residual of equation (1) (Figure 13). The energy spent on evaporation is lower in the south and west where surface temperatures are higher, while greater values have been computed in the north-east of Istria. Higher surface temperatures, in comparison with lower surface temperature, indicate that less energy must be spent to change water from liquid to water vapour (Figure 14). Učka and Ćićarija mountain ranges are covered with denser and healthier vegetation and are characterized by lower temperatures. Thus, more of the available energy will be used up in the evaporation process.

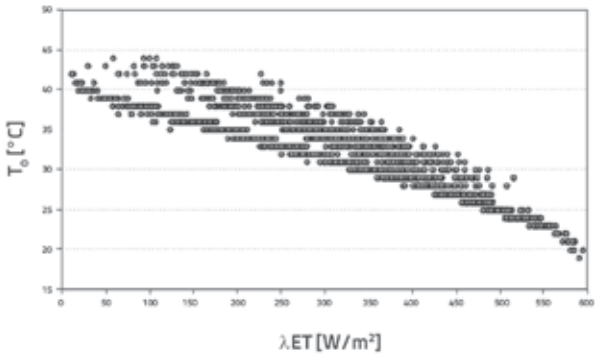

Figure 14. Relationship between latent heat flux and surface temperatures

The portion of the energy available for different processes in nature, especially for evapotranspiration, is dictated by the water content within the system: in humid areas more available energy will be spent on transpiration (higher λET values) while in drier areas the energy will largely be used for heating up the surface (higher H values). Therefore, the evaporative fraction, as the ratio of latent to available energy, is a good indicator of a hydrologic state of the system (Figure 15). In the north-east, the evaporative fraction is high which is an indication of a larger water content in the system. It also suggests that a larger portion of the available energy is spent on the ET process (more than 80 % at some locations). In the

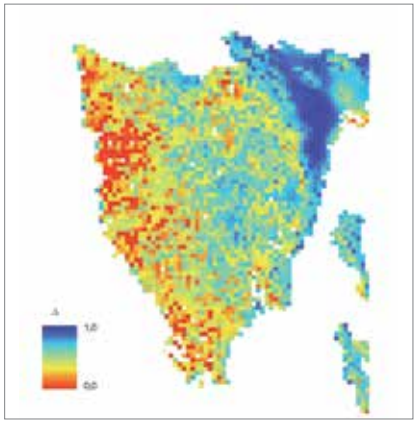

Figure 15. Evaporative fraction (5th August 1998)

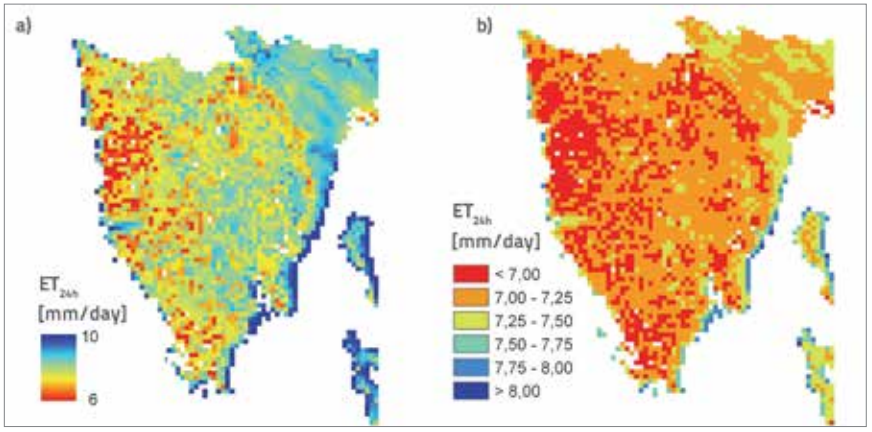

Figure 16. Actual daily evapotranspiration (5 August 1998): a) on a continuous values domain; b) classified into value classes

west and south of Istria, more available energy is spent on heating up the surface (lower evaporative fraction values).

Knowing the daily net evapotranspiration and evaporative fraction, the actual daily ET is estimated using the equation (19) (Figure 16).

Lowest actual daily ET values are characteristic for the driest parts of the area under study where water availability is at its minimum in comparison with the rest of Istria. Daily ET losses range from 6.5 – 7 mm on the west and south coast, to 7 – 7.25 mm in the central, north and north–east Istria. Extremely high ET values (in comparison with other pixels) detected in a narrow coastal zone (> 8 mm/day), especially in the east, are not an indicator of a high ET but a consequence of a very coarse spatial resolution of the satellite image. The spatial resolution of 1 km is not sufficient to accurately delineate sea from land. As a consequence, many coastal pixels contain mixed information on surface characteristics, resulting in unrealistically high ET values.

The ET depends on numerous factors, one of them being the surface temperature (Figure 17). Higher surface temperature is an indicator of a smaller soil moisture content and, hence, of a smaller ET. When available soil moisture decreases in subsurface soil (within the root zone), the stomata close up and reduce transpiration. Hence, the soil heats up faster and more of the available energy is used to rise the surface temperature.

Only two of the gauging stations selected in the analyzed area conduct evaporation measurements: Abrami and Pazin, both using the Class A evaporation pan. The comparison of an estimated actual daily evapotranspiration with the measured evaporation is shown in Table 2.

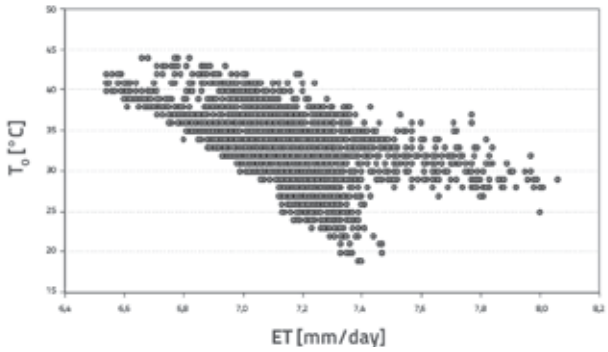

Figure 17. Relationship between actual daily evapotranspiration and surface temperature

The Class A evaporation pan estimates water losses by measuring evaporation from the free water surface. Such measurements are not representative for the influence of vegetation on water losses. The evaporation estimated using the evaporation pan represents a result of the combined influence of radiation, temperature, humidity and wind velocity on the evaporation process [8]. By applying empirical coefficients that compensate for the influence of transpiration, measurements can be associated with the referent ET. The resulting differences between the referent and actual ET are expected, because of different reflective characteristics of the water and vegetation. However, these differences are quite significant (1,83 mm i.e. 26 % at the Abrami station, and 1,38 mm i.e. 19,8 % at the Pazin station).

In the engineering practice, the most common methods are those that are used to estimate referent evapotranspiration. The referent evapotranspiration ET_R is the water lost through

Table 2. Actual daily evapotranspiration and measured evaporation (5th August 1998)

Station	z [m a.s.l.]	ET_{24h} [mm/day]	E [mm/day]	ΔET [%]
Abrami	85	7,03	5,2	26,0
Pazin	291	6,98	5,6	19,8

Table 3. Actual daily and referent evapotranspiration at meteorological gauging stations (5th August 1998)

Stations	z [m a.s.l.]	NDVI	ET_{24h} [mm/day]	ET_R [mm/day]	ΔET [%]
Abrami	85	0,66	7,03	6,09	-13,4
Celega	20	0,31	-	6,96	-
Cres	5	0,49	7,36	8,15	9,6
Ćepić	30	0,64	7,21	8,02	10,1
Labin	260	0,64	7,05	4,71	-33,3
Pazin	291	0,63	6,98	5,21	-25,3
Poreč	15	0,24	-	4,76	-
Pula	43	0,43	-	9,24	-
Pula aerodrom	63	0,58	7,17	7,93	9,6
Rijeka	120	0,49	-	7,51	-
Rovinj	20	0,57	7,30	6,41	-12,2

z: Ititude; ET_{24h}: actual daily evapotranspiration; ET_R: referent evapotranspiration; ΔET: difference between actual and referent evapotranspiration

evapotranspiration from the referent surface (grass cover with specific characteristics), and it defines atmospheric water demands, regardless of the crop cover, crop maturity and farming practices. When actual daily evapotranspiration measurements are not available, the referent daily evapotranspiration is calculated for the gauging station locations, using the FAO-56 Penmam Monteith method [8]:

$$ET_R = \frac{0,408 \cdot \Delta \cdot (R_n - G) + \gamma \cdot \frac{900}{T+273} \cdot u_2 \cdot (e_s - e_a)}{\Delta + \gamma \cdot (1 + 0,34 \cdot u_2)} \text{ [mm/day]} \qquad (20)$$

where R_n is the net radiation [MJ/m²day], G is the soil heat flux [MJ/m²day], γ is the psychrometric constant [kPa/°C], and T is the air temperature [°C]. Parameters e_s and e_a are the maximum and actual vapour pressures, respectfully [kPa], u_2 is the wind velocity at 2 m above the ground [m/s], while Δ represents the slope of the saturation vapour pressure temperature relationship [kPa/°C]. Since the FAO-56 Penman-Monteith method is also based on the energy balance approach, the actual daily ET is compared with estimated referent ET values at the discrete locations of the gauging stations (Table 3).

Differences between referent and actual daily ET are significant. The greatest differences have been recorded at the stations of Labin (33,3 %) and Pazin (25,3 %), both located at higher altitudes, in areas with a well developed relief. Differences are the smallest at stations Cres and Pula airport (9,6 %) and Ćepić (10,1 %), which are located in a more monotonous relief. The actual evapotranspiration could not be estimated at four stations in coastal area (Celega, Poreč, Pula, Rijeka) because the spatial resolution was too small.

6. Conclusions

The paper presents a new methodological approach to estimating evapotranspiration in this area, not only in terms of quantification but also in terms of spatial characteristics of the water balance component. Istria has been selected as the research area because of its significant hydrologic and climatologic heterogeneity, with pronounced karstic characteristics that additionally complicate the water balance analysis. The goal was to estimate evapotranspiration and its spatial distribution with minimum input data, taking into consideration numerous factors that influence the process of evapotranspiration, i.e. an attempt was made to gain an insight into the evaporation and transpiration water losses on a specific time scale. Estimated results were compared with evaporation measured at two meteorological gauging stations, and with the referent evapotranspiration calculated using the FAO-56 Penman Monteith method for 11 selected meteorological gauging stations with relevant measurements. Differences are significant: the greatest differences were found in colder parts located at higher altitudes, covered with dense vegetation, where a great amount of available energy is used in the process of evapotranspiration. In coastal area, where temperatures are higher and vegetation is scarce and dry, the evapotranspiration losses are smaller.

The approach presented in the paper is based on numerous assumptions, as needed to enable calculations. In that respect, instantaneous incoming shortwave and longwave radiations are assumed to be constant for the entire area. The surface temperature, as one of the most influential factors in the evapotranspiration process, is a function of solar radiation and reflective and thermal characteristics of the surface. The incoming radiation, both shortwave and longwave, is influenced by atmospheric constituents on its way through the atmosphere, and so it depends on atmospheric transmittance. Although the analyzed area is very heterogeneous, it is small enough to justify the assumption of uniformity of atmospheric conditions, as confirmed by incoming shortwave and longwave results calculated at the stations.

The value domain for sensible and latent heat fluxes is bounded by two boundary conditions defined as "hot" and "cold" pixels. The "hot" pixel is assigned to very dry terrain where the assumption of zero latent heat flux is valid, while the choice of the "cold" pixel is based on the minimum temperature gradient between the surface and the air. On wet terrains, the water vapour is released according to atmospheric demand, and the vertical temperature gradient is at its minimum. That leads to the sensible heat flux decrease and so, when it comes to wet terrains, i.e. the "cold" pixel, the assumption of sensible heat flux being equal to one is justified. The difference between temperature of the surface and the air is not based on actual measurements, but is calculated using the inverse sensible heat flux equation for boundary pixels. That introduces an additional uncertainty as well as the assumption of linear relationship between the air and surface temperatures, while the influence of vegetation on vertical change of temperature is neglected. However, unlike most other methods, this approach takes into consideration numerous factors that are of significance to evapotranspiration.

Knowing the net radiation, soil and sensible heat fluxes, the actual evapotranspiration estimation is based on the assumption that the daily variability of evaporative fraction can be neglected, which is not necessarily true. The evaporative fraction is inversely proportional to available energy ($R_n - G_0$) and so the slightest change in net radiation may cause a significant variation in the daily curve of the evaporative fraction, especially when ($R_n - G_0$) values are low (morning and evening, presence of clouds). During the day, the evaporative fraction does not change significantly, and the assumption of constant values is realistic. However, this does not apply to cloudy days. Clouds reduce the net radiation and hence the available energy. Depending on the temperature, humidity, wind velocity and difference between air and surface temperatures, the ($R_n - G_0$) must be equal to the sum of latent and sensible heat fluxes. A decrease in surface temperatures will induce decrease in the sensible heat flux more than in the latent heat flux, which will increase the evaporative fraction. In general, clouds cause changes in the heating of the surface as well as in energy availability on a daily time scale, which leads to diurnal variability of the evaporative fraction.

The comparison of spatial variation of surface temperature and actual daily ET shows that the spatial variability of the estimated actual daily ET can be considered realistic for the analyzed area. As expected, the ET value is smaller in parts with higher surface temperatures, and it increases with an altitude, while the surface temperature decreases. Although the estimated actual daily ET values are higher than the evaporation measured at Abrami and Pazin, one must bear in mind that the pan evaporation is often not representative for vegetated areas. Reasons for overestimating the actual daily evapotranspiration, in comparison with the measured evaporation and the calculated referent evapotranspiration, can be found in previously discussed assumptions, especially in the way the sensible heat is calculated. On the other hand, the referent evapotranspiration does not take into consideration the vegetation cover or reflective and thermal characteristics of the surface, but is based solely on climatologic parameters. Further research should place an emphasis on the choice of images in the context of spatial resolution as related to the size of the research area, as well as on calibration of the model with actual daily evapotranspiration measurements. Furthermore, an analysis of several images would give a valuable insight into the dynamics of evapotranspiration over longer time periods, which would contribute to better validation of the presented approach and its applicability in the area under study. The described approach for estimating the actual daily ET enables the ET estimation in areas where measurements are very scarce, as is the case with the Istrian peninsula.

Acknowledgments

The author wishes to thank the State Meteorological and Hydrological Service from Zagreb for their kind assistance and contribution in collecting the data, which enabled the research and publication of this paper.

REFERENCES

[1] Kundzewicz, Z.W.: Water problems of central and eastern Europe – a region in transition. Hydrological Sciences Journal, 46(6), pp. 883-896, 2001.

[2] Bonacci, O.: Ekohidrologija, Građevinsko-arhitektonski fakultet Sveučilišta u Splitu, Institut građevinarstva Hrvatske, Zagreb, 2003.

[3] Hipps, L. & Kustas, W.: Patterns and Organisation in Evapotranspiration (Chapter), Spatial Patterns in Catchment Hydrology: Observation and Modeling, eds. R. Grayson & G. Blöschl, Cambridge University Press, United Kingdom, pp. 105-122, 2000.

[4] Feddes, R.S. & Lenselink, K. J.: Evapotranspiration (Chapter), Drainage Principles and Applications, ed. H. P. Ritzema, International Institute for Land Reclamation and Improvementm Wageningen, The Netherlands, pp. 145-173, 1994.

[5] Jensen, M.E., Burman, R.D., Allen, R.G.: Evaporation and irrigation water requirements. ASCE Manual, 70, New York, USA, 1990.

[6] Vörösmarty, C.J., Federer, C.A., Schloss, A.L.: Potential evapotranspiration functions compared on US watersheds: Possible implications for global-scale water balance and terrestrial ecosystem modeling. Journal of Hydrology, 207, pp. 147-169, 1998.

[7] Baastiansen, W. G. M., Menenti, M., Feddes, R.A., Holtslag, A. A. M.: A remote sensing surface balance algorithm for land (SEBAL), Journal of Hydrology, 212-213, 1998.

[8] Allen, R. G.. Pereira, L. S., Raes, D., Smith, M.: Crop Evapotranspiration (Guidelines for Computing Crop Water Requirements), FAO Irrigation and Drainage Paper No. 56, Rome, Italy, 1998.

[9] Parodi, G. N.: AVHRR Hydrological Analysis System. Algorithms and theory – version 1.3, International Institute for Geo-information Science & Earth Observation (ITC), Enschede, The Netherlands, 2002.

[10] van de Griend, A. A. & Owe, M.: On the relationship between thermal emissivity and the normalized difference vegetation index for natural surfaces, International Journal of Remote Sensing, 14(6), pp. 1119-1131, 1993.

[11] Kidwell, K. B.: NOAA Polar Orbiter Data User's Guide, U.S. Department of Commerce, National Oceanic and Atmospheric Administration, Suitland, USA, 1998.

[12] Jang, J. D.: Evaluation of thermal-water stress of forest in southern Quebec from satellite images, PhD thesis, Department of Geomatics Sciences, Laboratorie de géomatique agricole at appliquée (GAAP), Centre de Recherche en Géomatique (CRG), Université Laval, Québec, Canada, 2004.

[13] Chen, T.S. & Ohring, G.: On the relationship between clear-sky planetary and surface albedos: a parametrization for simple energy balance climate models, Advances in Space Research, 6(5), pp. 141-144, 1985.

[14] Rao, C. R. N. & Chen, J.: Revised post-launch calibration of channels 1 and 2 of the Advanced Very High Resolution Radiometer on board the NOAA-14 spacecraft, NOAASIS, 1999. http://noaasis.noaa.gov/NOAASIS/ml/aboutn14vis.html

[15] Sauer, T. J. & Horton, R.: Soil heat Flux, Micrometeorology in Agricultural Systems, eds. J. L. Hartfield, J. M. Baker, American Society of Agronomy, Inc., Crop Science Society of America, Inc., Soil Science Society of America, Inc., Madison, Wisconsin, USA, pp. 131-154, 2005.

[16] Baastiansen, W. G. M.: Regionalization of surface flux densities and moisture indicators in composite terrain. A remote sensing approach under clear skies in Mediterranean climates, Doctoral thesis, Landbouwuniversiteit, Wageningen, The Netherlands, 1995.

[17] Garrat, J.R.: The Atmospheric Boundary Layer, Cambridge University Press, Cambridge, pp. 31, 1994.

[18] Raupach, M.R.: Simplified expressions for vegetation roughness length and zero-plane displacement as functions of canopy height and area index, Boundary Layer Meteorology, 71, pp. 211-216, 1994.

[19] Oberg, J. W. & Melesse, A. M.: Evapotranspiration dynamics at an ecohydrological restoration site: an energy balance and remote sensing approach, Journal of the American Water Resources Association, 42(3), pp. 545-807, 2006.

[20] Monteith, J. L. & Unsworth, M.H.: Principles of Environmental Physics (2nd edition), Butterworth-Heinemann Woburn, Massachusetts, 1993.

[21] Likso, T.: Procjena temperature zraka na 5 cm iznad tla na opservatoriju Zagreb-Maksimir, magistarski rad, Prirodoslovno-matematički fakultet Sveučilišta u Zagrebu, 2005.

[22] Crago, R. & Brutsaert, W.: Daytime evaporation and the self-preservation of the evaporative fraction and the Bowen ratio, Journal of Hydrology, 178(1-4), pp. 241-255, 1996.

[23] Nichols, W. E. & Cuenca, R. H.: Evaluation of the evaporative fraction for parameterization of the surface energy balance. Water Resources Survey, 29(11), pp. 3681-3690, 1993.

[24] Shuttleworth, W. J., Gurney, R. J., Hsu, A. Y., Ormsby, J. P.: FIFE: The variation in energy partition at surface flux sites, IAHS Publications, 186, pp. 67-74, 1989.

[25] Rubinić, J.: Vodni resursi i značajke kopnenih voda Istre u sušnim razdobljima – hidrološka studija, knjiga 1 (nepublicirano), Građevinski fakultet Sveučilišta u Rijeci, Rijeka, 2005.

[26] Gajić-Čapka, M., Patarčić, M., Perčec Tadić, M., Srnec, L., Zaninović, K.: Meteorološka podloga za Vodnogospodarsku osnovu Hrvatske, Državni hidrometeorološki zavod, Zagreb, 2002.

[27] Horvat, B.: Analiza prostorne strukture komponenti bilance voda na području hrvatskog dijela Istre, doktorska disertacija, Fakultet građevinarstva, arhitekture i geodezije Sveučilišta u Splitu, 2012.